Int. J. Electron. Commun. (AEÜ) 177 (2024) 155198

Contents lists available at ScienceDirect

International Journal of Electronics and Communications

journal homepage: www.elsevier.com/locate/aeue

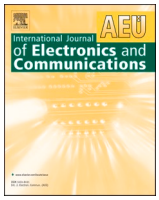

A magnetless filtering circulator with enhanced isolation bandwidth using mixed static and time-modulated resonators

Girdhari Chaudhary [a], Yongchae Jeong [b,*]

[a] JIANT-IT Human Resource Development Center, Jeonbuk National University, Jeonju-si, Jeollabuk-do 54896, Republic of Korea
[b] Division of Electronic Engineering, Jeonbuk National University, Jeonju-si, Jeollabuk-do 54896, Republic of Korea

ARTICLE INFO

Keywords:
Circulator
Mixed static and time-modulated resonators
Spatio-temporal modulation
Wideband isolation

ABSTRACT

This paper presents a design of magnetless microstrip line circulator with filtering response and extended isolation bandwidth through integration of mixed static and time-modulated resonators. By effectively coupling static resonators with time-modulated resonators, the proposed circulator can achieve a low forward transmission insertion loss with filtering response along with a wide isolation bandwidth. Wideband isolation can be achieved by creating two isolation nulls within the passband. For proof-of-concept, a microstrip line circulator is designed, simulated, and fabricated at center frequency of 1.75 GHz. The measured results are well agreed with simulations. The measurement results show maximum forward transmission insertion loss of 2.70 dB, in-band 20-dB isolation of 80 MHz, and in-band return losses better than 18 dB.

1. Introduction

Circulators play a pivotal role in various applications such as in-band full duplex system, simultaneous-transmit and receive (STAR) radar, and high power wireless base station transmitters [1]. Traditional circulators are constructed using ferrite magnetic materials [2,3]; however, they tend to be bulky, costly, and lack of compatibility with integrated circuit technology. Non-magnetic nonreciprocity has been explored through exploiting nonreciprocal properties of transistors [4,5]. Nevertheless, these techniques are plagued by limitations such as poor noise and power handling performances.

Recently, spatio-temporal modulation (STM) of time-varying circuits has been shown to be a remarkable approach to nonreciprocal circuits without use of magnets [6–9]. In [10], circulator has been demonstrated by integrating gyrator with non-reciprocal phase characteristics, which can be achieved through switching local oscillator of N-path filters. In [11,12], the spatio-temporally modulated circulators are demonstrated by connecting three rings of resonators in either Δ or *Y*-configuration. The subsequent works [13,14] demonstrated magnetless circulators using a film bulk acoustic resonator (FBAR), AIN MEMS filter and CMOS RF switches, respectively. Despite significant research efforts, the previously reported circulators have exhibited narrowband isolation and matching bandwidths, featuring only a single isolation null and single reflection pole. In recent works, coupling static and time-modulated resonators has shown to be effective approach for enhancing reverse isolation bandwidth without increasing number of time-modulated resonators [15]. In [16], microstrip line circulator is demonstrated using static and time-modulated resonators. However, the reverse isolation bandwidth was limited to only 60 MHz within the passband.

In this paper, a microstrip line circulator is demonstrated by utilizing mixed static and time-modulated resonators. By effectively integrating static resonators with time-modulated resonators, the proposed circulator exhibits a filtering forward transmission response, along with an improved reverse isolation bandwidth featuring two nulls.

2. Design theory

Fig. 1(a) shows the coupling diagram of the proposed circulator, which is composed of three identical branches arranged in *Y*-topology. Each branch is composed of a RF port, a static resonator, and a time-modulated resonator. By modulating three time-varying resonators with progressive phase shift of 120° in clockwise direction, the desired RF signal transmission occurs in clockwise direction, while reverse isolation is achieved in the opposite direction. Fig. 1(b) shows the circuit diagram of the proposed circulator, where static resonators (L_2,C_2) are coupled with time-modulated resonators (L_1, and $C_1(t)$) through inverters in each branch.

Fig. 1(c) shows the microstrip line implementation of the proposed

* Corresponding author.
E-mail address: ycjeong@jbnu.ac.kr (Y. Jeong).

https://doi.org/10.1016/j.aeue.2024.155198
Received 30 November 2023; Accepted 14 February 2024
Available online 16 February 2024

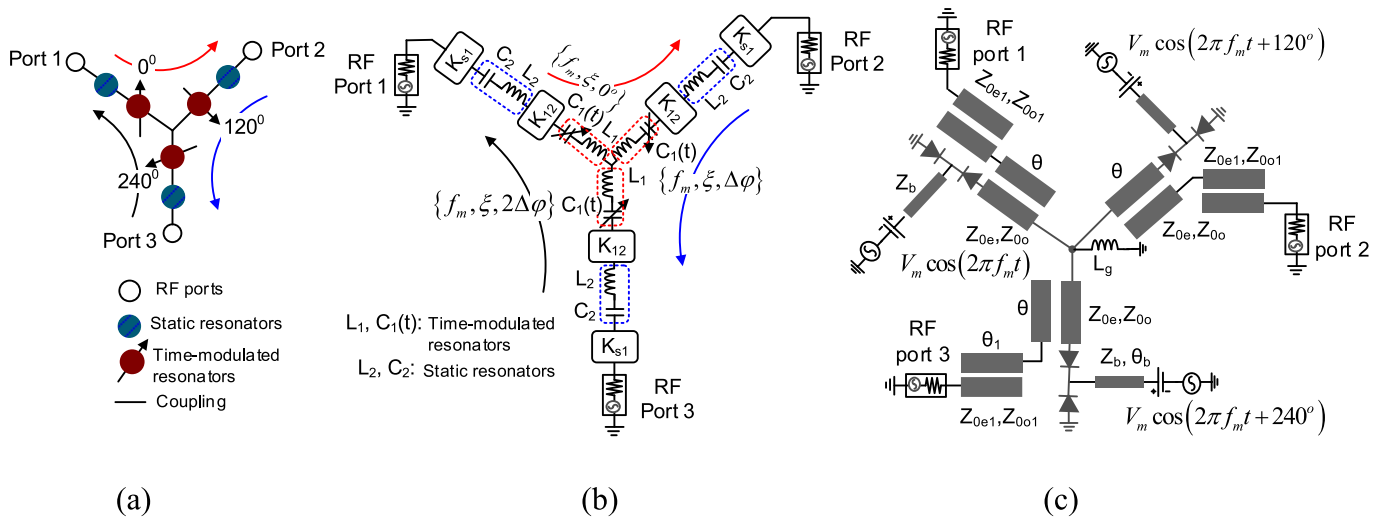

Fig. 1. Proposed circulator using mixed static and time-modulated resonators: (a) coupling diagram, (b) circuit diagram, and (c) microstrip line implementation of proposed circulator.

circulator comprising of three branches interconnected in *Y*-topology. Within each branch, the time-modulated resonators and static resonators are realized by using quarter-wavelength resonators loaded with varactors, and half-wavelength resonators, respectively. Each time-modulated resonator is interconnected with static resonator through coupled line with even/odd mode impedances of Z_{0e}/Z_{0o}, and electrical length of θ. Similarly, the static resonator is coupled to the RF port through coupled line with even/odd-mode impedances of Z_{0e1}/Z_{0o1}, and electrical length of θ_1. The time-varying capacitor is implemented by modulating the varactor diode. The modulation signal and dc-bias voltage are applied to time-varying resonator through transmission line with characteristics impedance of Z_b and electrical length of θ_b, simplifying modulation circuit design. To achieve circulator performance, the varactor diode of time-varying resonators is modulated according to following:

$$C_i(t) = C_0\left\{1 + \xi\cos\left[\omega_m t + (i-1)\frac{2\pi}{3}\right]\right\}, i = 1, 2, 3 \quad (1)$$

where C_0, ξ, and $\omega_m = 2\pi f_m$ are nominal static capacitance, modulation index, and modulation frequency, respectively [11].

In absence of modulation signal (*i.e.* static state), the circuit functions as reciprocal symmetrical three-port bandpass filter where input signal at port 1 is divided equally into port 2 and 3 (*i.e.* $|S_{21}| = |S_{12}| = |S_{31}| = |S_{13}| = 2/3 \approx -3.52$ dB). Upon the application of modulation signal, time-modulated resonator generates intermodulation (IM) products resulting from the RF and modulation signal mixing, which allow transmission with different distinct transmission phases. When RF signal at operating frequency ω_0 is applied to port 1, IM products are generated at $\omega_0 \pm k\omega_m$ (where $k = \cdots, -2, -1, 0, +1, +2, \cdots$) with distinct phase delays resulting from interaction of RF and modulation signal through time-modulated resonators [7,11]. After traveling through subsequent time-modulated resonator, the existing IM products undergo a second time mixing with modulation signal. The circulator can be designed in such a way that the powers at IM products at output port 2 can be added in phase, while the powers at IM products at output port 3 can be added 180° out of phase. With appropriate selection of modulation parameters, the powers at IM products can be constructively (0° in phase) combined at the RF carrier frequency, resulting minimum forward transmission loss (*i.e.* $|S_{21}| = |S_{32}| = |S_{13}| \approx 1$). Conversely, the powers at IM products are added up destructively (180° out of phase) in the reverse direction to create high reverse isolation (*i.e.* $|S_{12}| = |S_{23}| = |S_{31}| \approx 0$).

Parametric studies on modulation parameters have been carried out to optimize circulator performance. For the purpose of parametric studies, the SPICE model of varactor diode SMV 1233-079LF from Skyworks is used. The dc-bias voltage V_{dc} of 3.10 V is provided for each

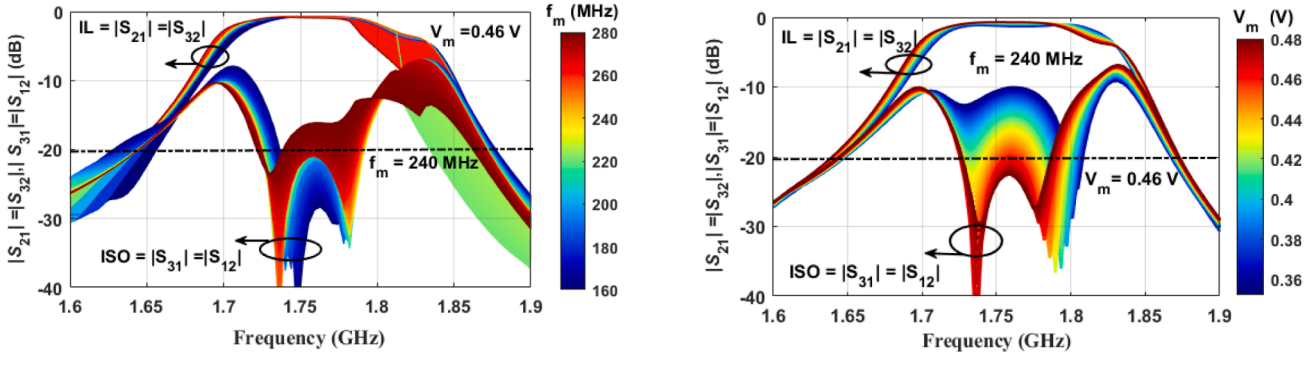

Fig. 2. Simulation results of the proposed circulator according to modulation parameters: (a) modulation frequency f_m and (b) modulation amplitude V_m. Circuit parameters of circulator: $Z_{0e} = 53\ \Omega$, $Z_{0o} = 35\ \Omega$, $\theta = 23°$, $Z_{0e1} = 127\ \Omega$, $Z_{0o1} = 70\ \Omega$, $\theta_1 = 69°$, $Z_b = 92$, and $\theta_b = 63°$. Electrical lengths of microstrip lines are defined at 1 GHz.

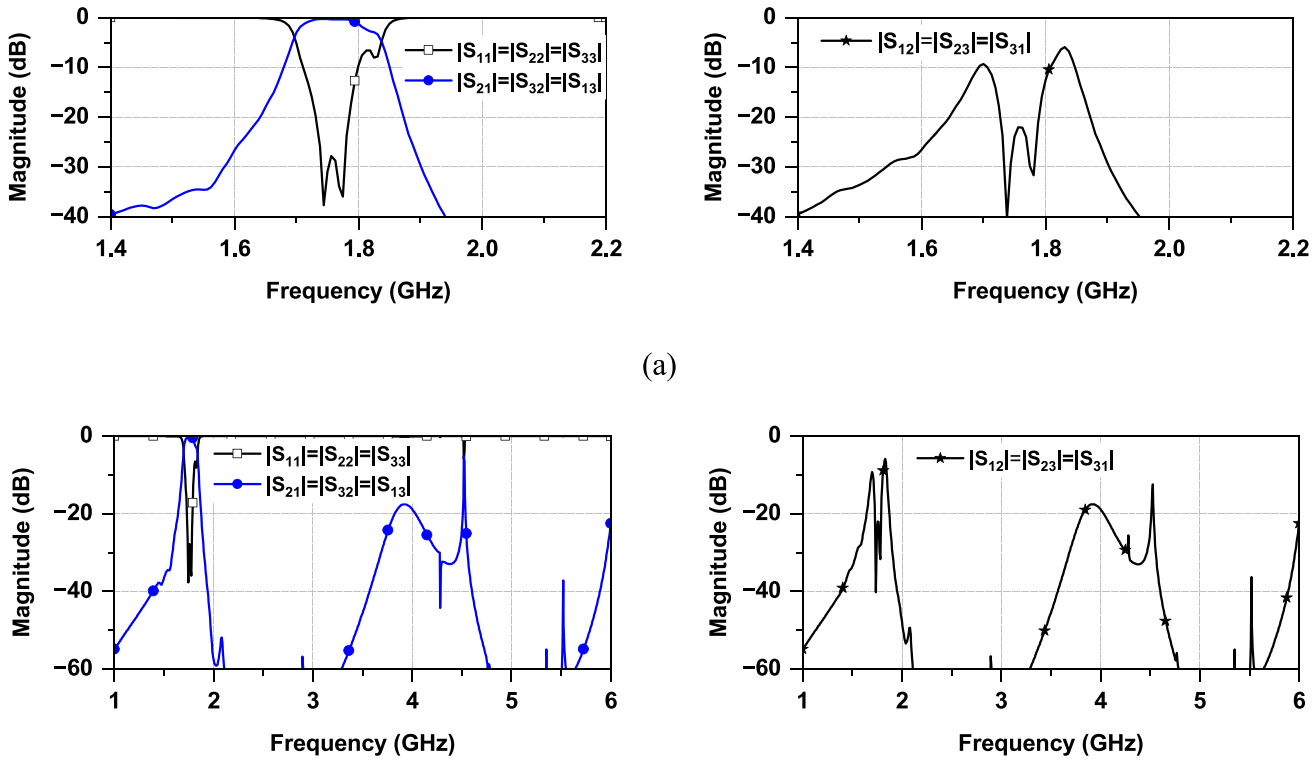

Fig. 3. Simulated results of the proposed circulator with modulation parameters of $f_m = 240$ MHz, $\Delta\varphi = 120°$ and $V_m = 0.46$ V: (a) narrowband frequency response and (b) wideband frequency response.

varactor diode. Fig. 2 shows the simulation results of the proposed circulator by sweeping modulation frequency $f_m = 160$ MHz to 280 MHz and modulation amplitude $V_m = 0.30$ V to 0.48 V. To effectively illustrate the parametric sweeping results, data visualization techniques such as line plots have been employed. On y-axis, amplitudes of *S*-parameters ($|S_{21}| = |S_{32}| = |S_{13}|$, $|S_{12}| = |S_{23}| = |S_{31}|$) are depicted, corresponding to frequencies plotted on the x-axis. Curves representing different modulation parameters such as f_m and V_m are distinguished by using different colors, as indicated in the color bar on the right side. This visualization approach enables designers to observe how *S*-parameters change under different selection of modulation parameters. Results show that two distinct nulls observed in reverse isolation. As seen from Fig. 2(a), a notably higher reverse isolation (such as >28 dB) at RF center frequency can achieved, when modulation frequency $f_m = 160$ MHz and $V_m = 0.46$ V, however, isolation bandwidth is relatively narrower. Conversely, a lower reverse isolation (such as >15 dB) at center frequency is observed when modulation frequency $f_m = 280$ MHz. As shown in Fig. 2(b), higher modulation amplitude V_m can achieve higher

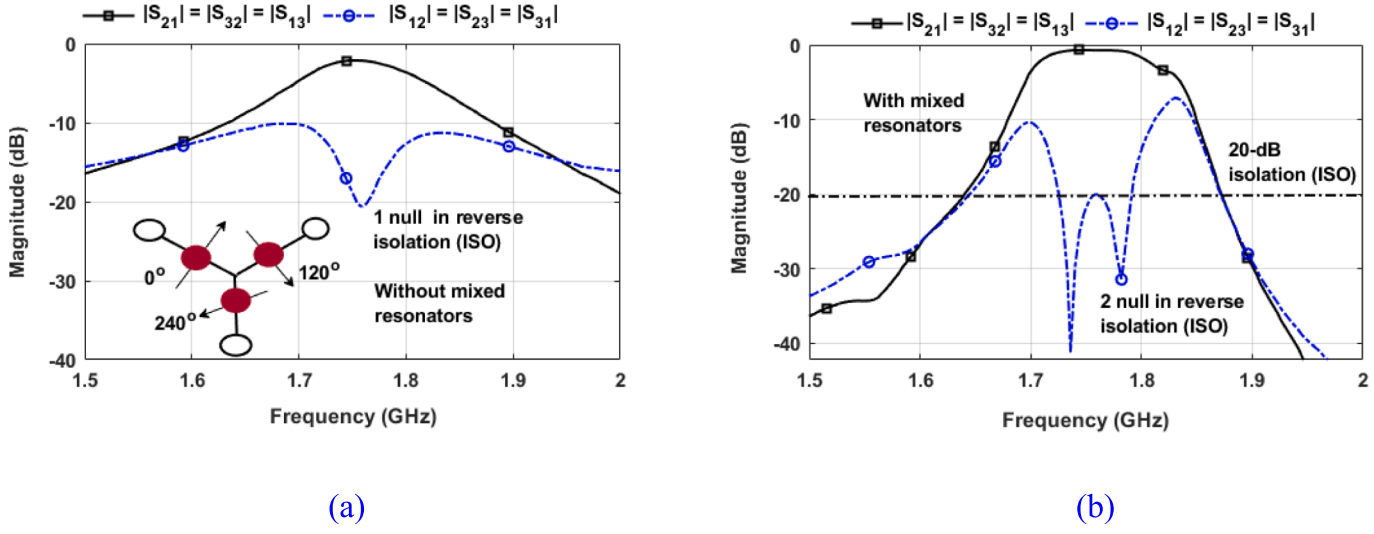

Fig. 4. Simulation results of proposed circulator with/without static resonators: (a) without mixed resonators and (b) with mixed static and time-modulated resonators.

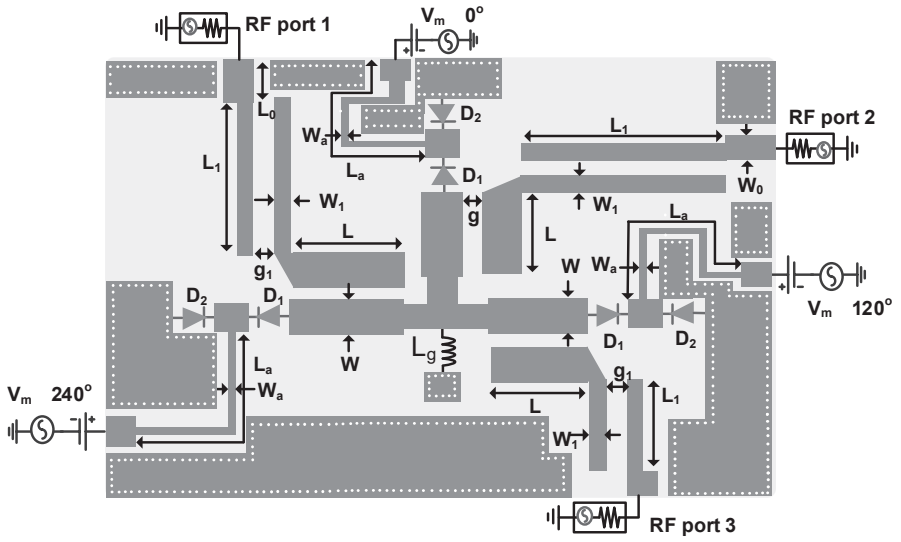

Fig. 5. Physical layout of fabricated circulator with dimensions: W = 2.9, g = 0.12, L = 15, W_1 = 0.55, g_1 = 0.55, L_1 = 40, W_0 = 2.4, L_0 = 3, W_a = 0.9, L_a = 36 and L_g = 100 nH. Varactor diode: SMV 1233-079LF from Skyworks. Unit: millimeter.

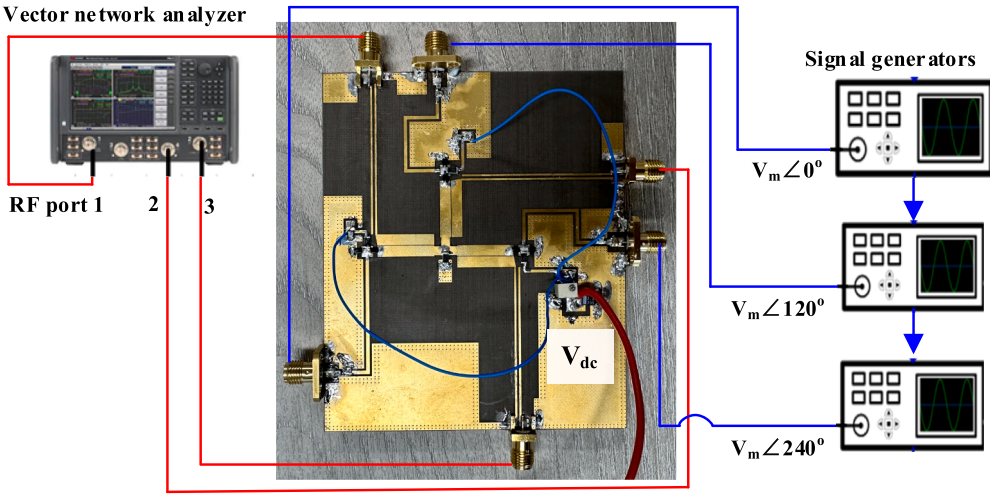

Fig. 6. Photograph of fabricated circulator with measurement setup.

reverse isolation with the cost of an increased forward transmission insertion loss (IL) and reduced reverse isolation bandwidth. Based on these parametric studies, the optimum performance of the proposed circulator such as forward transmission IL < 0.80 dB and return loss > 20 dB within passband, and reverse isolation > 20 for 90 MHz bandwidth; can be achieved when modulation frequency f_m = 240 MHz and V_m = 0.46 V.

Fig. 3 shows the simulated narrowband and wideband frequency response of the proposed circulator when modulation frequency f_m = 240 MHz, $\Delta\varphi = 120^\circ$, and V_m = 0.46 V are applied. As seen from these results, the proposed circulator provides filtering response in forward direction where attenuation is higher than 18 dB extending DC to 1.62 GHz and 1.85 GHz to 4.60 GHz. Likewise, the transmission IL is nearly equal to 0.80 dB whereas reverse isolation is higher than 20 dB within passband. Good impedance matching (return loss > 15 dB) is achieved within passband.

Fig. 4(a) shows the simulation results of circulator without static resonators. As seen from Fig. 4(a), when no static resonators are coupled with time-modulated resonators, only one null occurs in reverse isolation, providing narrowband reverse isolation bandwidth. Fig. 4(b) shows the simulation results of the proposed circulator where mixed static and time-modulated resonators are used. As seen from Fig. 4(b), two distinct nulls in reverse isolation are observed when mixed static resonators are coupled with time-modulated resonators, showing the wideband and high reverse isolation without increasing number of time-modulated resonators.

3. Experimental results

For proof-of-concept, the proposed circulator is designed, simulated, and fabricated at center frequency of 1.75 GHz using Taconic substrate with a dielectric constant of 2.2 and thickness of 0.78 mm. Fig. 5 presents the physical layout of the fabricated non-magnetic circulator. The shunt inductor L_g is placed at center of *Y*-topology to provide a dc return path. The electromagnetic co-simulation was performed using ANSYS HFSS and Keysight ADS in conjunction with a large signal scattering harmonic balance (HB) module. Fig. 6 shows the photograph of fabricated circulator with measurement setup.

Fig. 7 shows the simulated and measured results of circulator. The reverse-biased dc-voltage of 3.10 V is applied to varactors diodes. Based on previously discussed parametric studies, the modulation parameters of f_m = 235 MHz and V_m = 0.46 V are chosen to achieve optimum

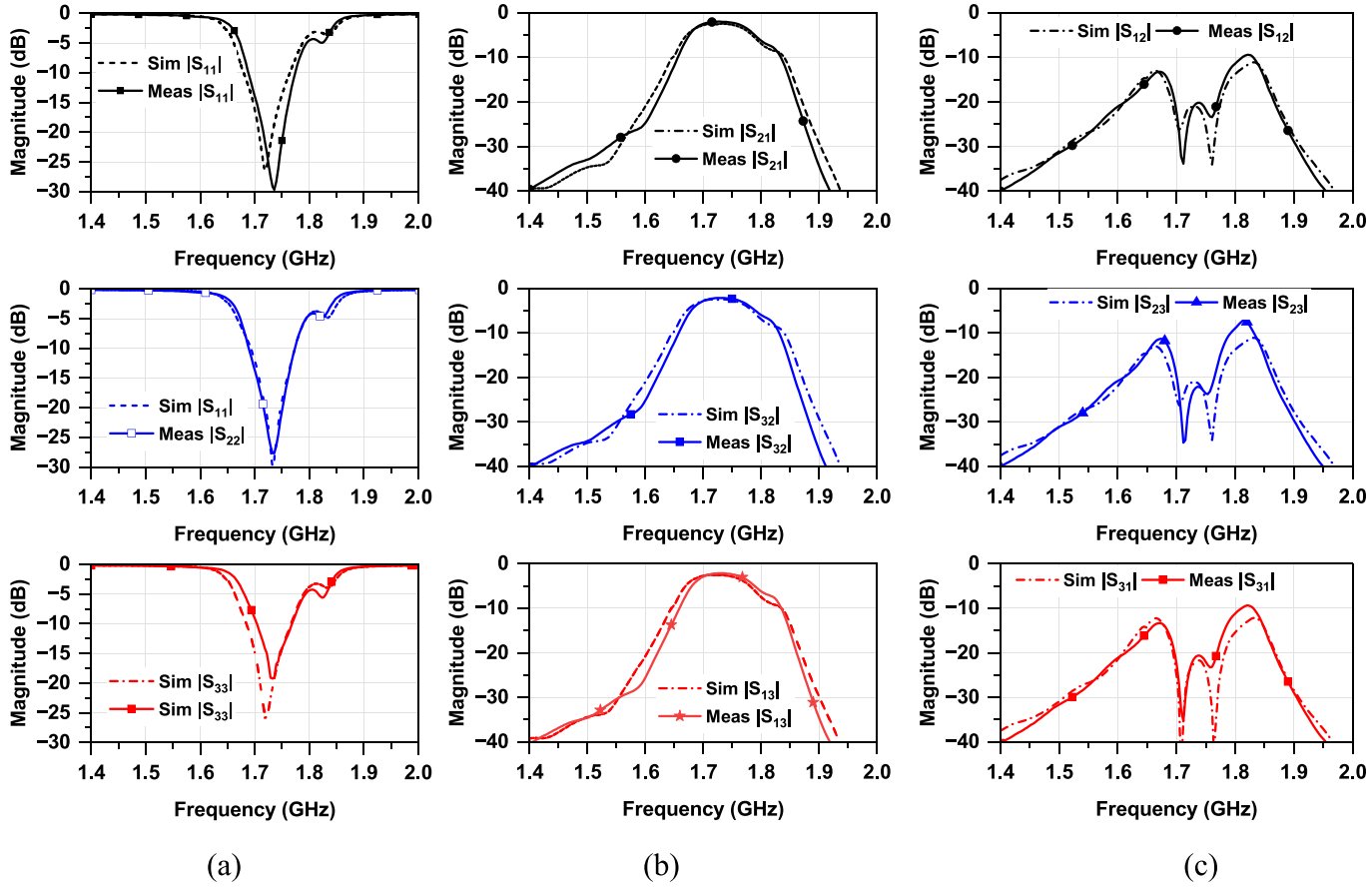

Fig. 7. Simulated and measured results of the proposed circulator: (a) return losses ($|S_{11}|$, $|S_{22}|$, $|S_{33}|$), (b) forward transmission insertion loss ($|S_{21}|$, $|S_{32}|$, $|S_{13}|$), and (c) reverse isolation ($|S_{12}|$, $|S_{23}|$, $|S_{31}|$).

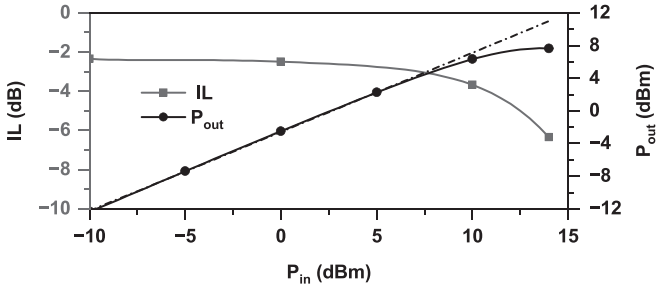

Fig. 8. Measured power handling of the proposed circulator.

circulator performance. The measured results are well agreed with simulations. The measured forward transmission IL is 2.70 dB with 3-dB transmission bandwidth of 130 MHz. The IL in forward direction is mainly due to parasitic resistance of varactor diode. Notably, the measured in-band reverse isolation is better than 20 dB over the frequency range of 1.70 GHz to 1.78 GHz, providing 20 dB reverse isolation bandwidth of 80 MHz. Furthermore, reverse isolation characteristics exhibit two distinct nulls. The measured in-band reflection is below −18 dB, showing wideband good matching characteristics.

The power handling capability of the proposed circulator is mainly constrained by the nonlinearity of varactor diodes. Fig. 8 shows the measured 1-dB compression point (P_{1dB}) using single-tone RF signal at 1.75 GHz. The forward transmission IL ($|S_{21}|$) is degraded when input power (P_{in}) is higher than 10 dBm, providing P_{1dB} is approximately equal to 10.5 dBm.

Circulators should fulfill various performances criteria, including a low transmission IL, high return loss (RL), and high reverse isolation over the wide frequency bandwidth. Nevertheless, achieving these diverse performances concurrently can be challenging. To address this challenge, (FoM) can be defined as (2), which takes into account various performance aspects of the circulator.

$$\text{FoM} = \frac{BW_{20dB\_ISO}(MHz)}{BW_{3dB\_IL}(MHz)} \times \frac{RL(dB)}{IL(dB)} \tag{2}$$

where BW_{3dB_IL} and BW_{20dB_ISO} are 3-dB forward transmission passband bandwidth and 20-dB reverse isolation bandwidth.

Table 1 compares the performance of the proposed circulator with previously reported works. As seen from Table 1, the previously reported circulators in [7,10,12–15] exhibits a narrow 20-dB reverse isolation bandwidth (<23 MHz) with one null, except [] [16]. The work [16] demonstrated circulator having isolation with two nulls, however, 20-dB isolation bandwidth is only 60 MHz and FoM = 3.80. In contrast, this work demonstrated circulator with relatively low forward IL (<2.70 dB) and wider 20-dB reverse isolation bandwidth with two nulls. In addition, the proposed work achieved the highest FoM among previously reported non-magnetic circulators.

4. Conclusion

In this work, a non-magnetic circulator with filtering response and wide reverse isolation bandwidth is demonstrated using mixed static and time-modulated resonators. By effectively integrating static resonators with time-modulated resonators the reverse isolation bandwidth circulator can be enhanced, while simultaneously achieving a relatively low transmission insertion loss. The enhancement of reverse isolation bandwidth is facilitated by the creation of two distinctive nulls. For

Table 1
Performance comparison between this work and previously reported circulators.

	[6]	[9]	[11]	[12]	[13]	[14]	[16]	This work
Configuration	Differential	Differential	Single-ended	Single-ended	Single-ended	Single-ended	Single-ended	**Single-ended**
Technology	Lumped LC	Microstrip	Lumped LC	Lumped LC	FBAR	AIN MEMS	Microstrip	**Microstrip**
f_0 (GHz)	1	1.99	0.130	1	2.50	1.20	0.825	**1.75**
IL (dB)	2	4.80	9	3.3	11	12	1.70	**2.70**
RL (dB)	>20	>7	>4	>10.8	>8.5	>10	>14	**>18**
BW_{3dB} (dB)	80	40	16	80	10	3	130	**130**
BW_{ISO} (MHz)	23	20	9	20	4	NA	60	**80**
No. of ISO nulls	1	1	1	1	1	1	2	**2**
Circuit size (λ_g^2/mm^2)	$(0.09 \times 0.07)\lambda_g^2$ (27 × 22) mm^2	NA	$(0.01 \times 0.01)\lambda_g^2$ (24 × 23) mm^2	$(0.05 \times 0.04)\lambda_g^2$ (15 × 12) mm^2	$(0.1 \times 0.07)\lambda_g^2$ (12 × 8) mm^2	NA	$(0.37 \times 0.37)\lambda_g^2$ (135 × 135) mm^2	$(0.55 \times 0.45)\lambda_g^2$ (95 × 77) mm^2
FoM/NCS (λ_g^2)	2.88/0.0063 = 457.14	NA	0.25/0.0001 = 2500	0.82/0.002 = 410	0.31/0.007 = 44.28	NA	3.80/0.1369 = 27.75	4.10/0.2475 = 16.57

BW_{3dB}: 3-dB transmission passband bandwidth, BW_{ISO}: 20-dB reverse isolation (ISO) bandwidth. ISO = isolation.
λ_g: Guided wavelength at operating center frequency f_0. NCS: total network circuit size in terms of guided wavelength.

experimental validation, a prototype of microstrip line circulator is designed and fabricated at center frequency of 1.75 GHz. The proposed circular can be applied for self-interference cancellation in full duplex communication systems.

CRediT authorship contribution statement

Girdhari Chaudhary: Writing – review & editing, Writing – original draft, Validation, Investigation, Conceptualization. **Yongchae Jeong:** Writing – review & editing, Visualization, Supervision, Project administration, Funding acquisition, Conceptualization.

Declaration of competing interest

The authors declare that they have no known competing financial interests or personal relationships that could have appeared to influence the work reported in this paper.

Data availability

Data will be made available on request.

Acknowledgment

This research was supported by National Research Foundation of Korea (NRF) grant funded by Korea Government (MSIT: Ministry of Science and ICT) (No. RS-2023-00209081) and in part by Basic Science Research Program through the NRF grant funded by Ministry of Education (2019R1A6A1A09031717).

References

[1] Kolodziej KE, Perry BT, Herd JS. In-band full-duplex technology: Techniques and systems survey. IEEE Trans Microwave Theory Techn 2019;67(7):3025–41.
[2] Fay CE, Comstock RL. Operation of the ferrite junction circulator. IEEE Trans Microwave Theory Tech 1965;13(1):15–27.
[3] O'Neil BK, Young JL. Experimental investigation of a self-biased microstrip circulator. IEEE Trans Microwave Theory Techn 2009;57(7):1669–74.
[4] Tanaka S, Shimomura N, Ohtake K. Active circulators: The realization of circulators using transistors. Proc IEEE 1965;53(3):260–7.
[5] Ayasli Y. Field effect transistor circulators. IEEE Trans Mag 1989;25(5):3242–7.
[6] Kord A, Sounas DL, Alu A. Pseudo-linear time-invariant magnetless circulators based on differential spatiotemporal modulation of resonant junctions. IEEE Trans Microwave Theory Techn 2018;66(6):2731–45.
[7] Wu X, Liu X, Hickle MD, Peroulis D, Gomez-Dıaz JS, Alvarez-Melcon A. Isolating bandpass filters using time-modulated resonators. IEEE Trans Microwave Theory Techn 2019;67(6):2331–45.
[8] Alvarez-Melcon A, Wu X, Zang J, Liu X, Gomez-Dıaz JS. Coupling matrix representation of nonreciprocal filters based on time modulated resonators. IEEE Trans Microwave Theory Techn 2019;67(12):4751–63.
[9] Chen Z, Zhou C, Wu W. Magnetless microstrip circulators based on differential spatiotemporal modulation of resonators. Int J RF Microwave Comput Aided Eng 2022;32(3):1–8.
[10] Reiskarimian N, Krishnaswamy H. Magnetic-free non-reciprocity based on staggered commutation. Nature Commun 2016;7:11217.
[11] Estep NA, Sounas DL, Alu A. Magnetless microwave circulators based on spatiotemporally modulated rings of coupled resonators. IEEE Trans Microwave Theory Techn 2016;64(2):502–18.
[12] Kord A, Sounas DL, Alu A. Magnet-less circulators based on spatiotemporal modulation of bandstop filters in a delta topology. IEEE Trans Microwave Theory Techn 2018;66(2):911–26.
[13] Torunbalci M, Odelberg TJ, Sridaran S, Ruby RC, Bhave SA. An FBAR circulator. IEEE Microwave Wireless Components Letters 2018;28(5):395–7.
[14] Xu C, Piazza G. Magnet-less circulator using AIN MEMS filters and CMOS RF switches. J Microelectromech Syst 2019;28(3):409–18.
[15] Chaudhary G, Jeong Y. Nonreciprocal bandpass filter using mixed static and time-modulated resonators. IEEE Microwave Wirel Compon Lett 2022;32(4):297–300.
[16] Wu X, Nafe M, Liu X. A magnetless microstrip filtering circulator based on coupled static and time-modulated resonators. IEEE-MTTS Int Microwave Symp 2020: 948–51.